Indirect Boundary Element Method Applied to Generalized Microstripline Analysis with Applications to Side-Proximity Effect in MMIC's

Keren Li and Yoichi Fujii, *Member, IEEE*

***Abstract*—A novel analysis of the electrical properties of the microstrip-like structures with generalized configuration by means of the indirect boundary element method (BEM) is proposed. In this method, the basic boundary-integral equation is derived by choosing an appropriate fundamental solution and the numerical calculation is done by considering the root-singularity of boundary distribution on the strip conductor. As an application, the proximity effects in MMIC's are calculated. By curve-fitting, the numerical results are expressed in a polynomial suitable for CAD of MMIC's.**

I. Introduction

RECENT developments in the field of monolithic microwave integrated circuits (MMIC's) permit us to design and to construct broadband circuits with low cost, high performance, small sizes, light weight and high reliability [1]. The lines interconnecting the devices in the MMICs are usually microstriplines (MSL) and coplanar waveguides (CPW). In highly integrated circuits, the "proximity" effects arise in MMICs as shown in Figs. 1(a) and (b), as is pointed out by Pucel [2]. Fig. 1(a) shows a configuration with an interaction between the lines (as a typical case, between the line and the ground plane). Fig. 1(b) shows a configuration in which changes of the characteristics arise when the conductor strip of MSL is approaching to the edge of a finite dielectric substrate (a chip). In this paper, this change is called the side-proximity effect. For both cases of Fig. 1(a) and (b), the analysis of the proximity effect is necessary for the accurate design of MMIC's. The effect as shown in Fig. 1(a) has been analyzed by means of the rectangular boundary-division-method proposed by one of the authors [3]. However, the side-proximity effect is difficult to be analyzed with this method and even with the well-known methods such as the conformal mapping techniques and the spectral domain method [4], because these structures have special configurations and special boundaries.

Manuscript received October 3, 1988; revised July 18, 1991.

K. Li is with the Department of Electronic Engineering, University of Electro-Communications, 1-5-1 Chofugaoka, Chofu-shi, Tokyo 182, Japan.

Y. Fujii is with the Institute of Industrial Science, University of Tokyo, 22-1 Roppongi-7, Minato-ku, Tokyo 106, Japan.

IEEE Log Number 9104769.

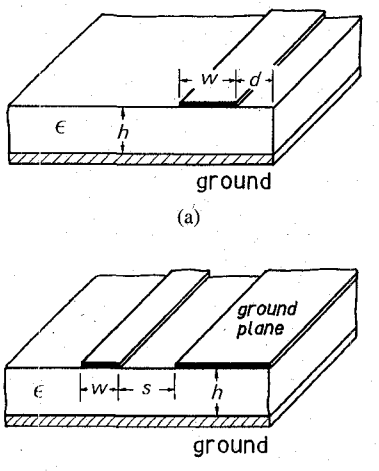

Fig. 1. "Proximity" effect in MMIC's. (a) Due to a ground plane. (b) Side-proximity effect.

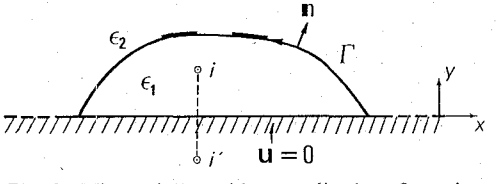

Fig. 2. Microstripline with generalized configuration.

In this paper, we propose a new method of analysis based on the indirect boundary element method (BEM) for microstriplines with generalized configuration as shown in Fig. 2. First, a simple boundary integral equation is derived by choosing an appropriate set of fundamental solutions, the square-root-singularity in the boundary distribution on the strip conductor is removed by an appropriate transformation and then the numerical analysis is carried out with high accuracy and with less CPU time.

As an application, the proximity effect in the MMIC is analyzed and by the curve-fitting, the numerical results for 50 Ω and 75 Ω lines with GaAs-substrate are given in polynomials suitable for CAD of the MMIC's.

II. Indirect BEM Analysis

The boundary element method (BEM) [5] is a numerical technique consisting of the following steps:

1) Transforming the ordinary differential equation into a boundary-integral equation.

2) Dividing the boundaries as in the case of the division of region in finite element method (FEM). The boundary integral equation is divided into a set of linear equations of the boundary values at the nodes on the finite discrete boundary.

3) The boundary values are obtained by numerically solving the linear equations.

The number of the data processed in the BEM is small but the accuracy is generally much higher than that in FEM. This is because the BEM makes the discretization only on the boundary, not over the region. So the BEM is applicable to a problem which has infinite regions or singularities to which the FEM is difficult to be applied [5]–[10].

In order to apply the BEM to the analysis of the side-proximity effect which appears in a structure as shown in Fig. 1(b), we first derive a boundary integral equation for the generalized MSL configuration. As shown in Fig. 2, there are two regions, finite and infinite. The quasi-TEM wave approximation is adopted to characterize this line because the dimensions in MMIC's are much smaller than the operating microwave wavelength [3], [11]. Using this approximation and letting $u(x, y)$ be a potential distribution function in the cross section of line, we solve an equivalent two-dimensional boundary value problem as shown in Fig. 3(a) and obtain u as

$$\nabla^2 u = \left(\frac{\partial^2}{\partial x^2} + \frac{\partial^2}{\partial y^2}\right) u = 0 \qquad \text{in } \Omega \tag{1a}$$

$$u = \bar{u} \qquad \text{on } \Gamma_1 \tag{1b}$$

$$q = \partial u/\partial n = \bar{q} \qquad \text{on } \Gamma_2 \tag{1c}$$

where the variables with bar denote the values on the boundaries. The boundary integral equation for (1a) is given [5]–[10] by the equation as

$$\tfrac{1}{2}u_i + \int_\Gamma uq^*\, d\Gamma = \int_\Gamma qu^*\, d\Gamma \qquad \text{for point } i \text{ on } \Gamma \tag{2a}$$

$$\nabla^2 u^* + \delta(i) = 0 \tag{2b}$$

where δ is Dirac's delta-function and u^* and q^* are the fundamental solutions of this system.

In the same way, the boundary integral equation for each region shown in Fig. 3(b) is solved. On the boundary Γ_I between two regions, the boundary conditions are given as follows:

$$u^{(1)} = u^{(2)} = u(I) \qquad \text{on } \Gamma_I \tag{3a}$$

$$\epsilon_1 q^{(1)} + \epsilon_2 q^{(2)} = -\sigma \qquad \text{on } \Gamma_I. \tag{3b}$$

where the so-called indirect boundary variable σ means the distribution of free charge density on the boundary Γ.

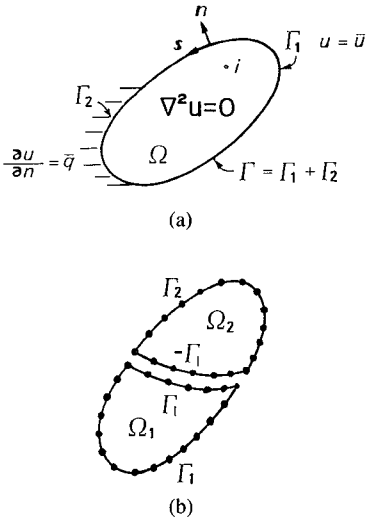

Fig. 3. (a) Two-dimensional boundry value problem. (b) Boundary value problem with two regions.

Starting from (2), q is substituted by the indirect boundary variable σ in (3b) by using the boundary conditions (3a) and (3b). Then by using the indirect boundary method and by taking the outer boundaries to infinity, a boundary-integral equation for u and σ on the intermediate boundary Γ_I is derived as follows:

$$\epsilon_I u(I)_i + \Delta\epsilon \int_{\Gamma_I} u(I) q^*\, d\Gamma = -\int_{\Gamma_I} \sigma u^*\, d\Gamma \qquad \text{for the point } i \text{ on } \Gamma_I \tag{4}$$

where $\epsilon_I = (\epsilon_1 + \epsilon_2)/2$ and $\Delta\epsilon = (\epsilon_1 - \epsilon_2)$.

In the case of the problem as shown in Fig. 2, we define the fundamental solution u^* in the semi-infinite region as follows:

$$u^* = \frac{1}{2\pi}\ln\frac{1}{r} - \frac{1}{2\pi}\ln\frac{1}{r'} = \frac{1}{2\pi}\ln\frac{r'}{r}, \tag{5a}$$

where

$$r = \sqrt{(x - x_i)^2 + (y - y_i)^2}$$

and

$$r' = \sqrt{(x - x_i)^2 + (y + y_i)^2}. \tag{5b}$$

The boundary integrals on all the boundaries except the intermediate boundary Γ_I vanish. Thus the boundary-integral equation is given only on Γ_I as follows:

$$\epsilon_I u_i + \Delta\epsilon \int_{\Gamma_I} uq^*\, d\Gamma = -\int_{\Gamma_I} \sigma u^*\, d\Gamma \qquad \text{for point } i \text{ on } \Gamma_I. \tag{6}$$

From this boundary-integral equation (6), a set of linear equations is obtained by dividing the boundaries into a set of finite linear elements and by taking the linear approx-

imation both for the boundary division and for the boundary distributions u and σ as follows:

$$\epsilon_I u_i + \Delta\epsilon \sum_{j=1}^{N} \hat{H}_{ij} u_j = -\sum_{j=1}^{N} \hat{G}_{ij}\sigma_j \quad (i = 1, \cdots, N), \tag{7}$$

where $\hat{H}$ and $\hat{G}$ are the coefficient matrices determined by (6). Using the expression for the coefficient matrices $\boldsymbol{H}$ and $\boldsymbol{G}$, (7) can be rewritten in a simple form as follows:

$$\boldsymbol{Hu} = \boldsymbol{G}\sigma. \tag{8}$$

where

$$H_{ij} = \begin{cases} \epsilon_I + \Delta\epsilon\hat{H}_{ii} & i = j \\ \Delta\epsilon\hat{H}_{ij} & i \neq j \end{cases} \quad \text{and} \quad G_{ij} = -\hat{G}_{ij}. \tag{9}$$

The coefficient matrices $\boldsymbol{H}$ and $\boldsymbol{G}$ are derived analytically as are shown in Appendix I.

The MSL has square-root-singularities in the distribution since the indirect boundary variable σ is the distribution of free charge density on the boundary Γ. So a serious computational error may take place if the distribution of σ is calculated directly by numerical computation. In this method of numerical computation, therefore, we transform σ as follows:

$$\sigma(x) = \frac{\sigma'(x)}{\sqrt{1 - (2x/w)^2}}, \tag{10}$$

where w is the width of conductor strip. By using this transformation, the computational error can be avoided because the integral of $\sigma(x)$ is convergent for finite values of $\sigma'(x)$. The discretization of $\sigma'(x)$ is also carried out for $\sigma(x)$. Thus a set of linear equations for σ' in (9) is given as follows:

$$\boldsymbol{Hu} = \boldsymbol{G}'\sigma'. \tag{11}$$

The coefficient matrix $\boldsymbol{G}'$ is numerically obtained (see Appendix II).

From the physical requirement, the distributions u and σ' in (10) must satisfy the boundary conditions as follows:

$$u = V_0 \quad \text{on the strip conductor, and} \tag{12a}$$

$$\sigma' = 0 \quad \text{except on the strip conductor.} \tag{12b}$$

It should be noted that the indirect boundary distribution σ' in (12b) can be calculated only on the conductor strip. This is the reason why the indirect BEM, instead of the conventional BEM, is utilized in this paper.

III. Analysis of Side-Proximity Effect

The method proposed above is applicable to analyze the side-proximity effect. First, the coordinates of a microstrip structure as shown in Fig. 1(b) are defined as shown in Fig. 4(a). The boundary Γ is divided into four parts. Numbers of each element are N_1, N_2, N_3 and N_4, respectively, and $N = N_1 + N_2 + N_3 + N_4$. At the non-smooth points on the boundary, two neighboring points necessary for the calculation are taken on both sides of this point. By the discretization and by using the transformation in (10), a set of linear equations as (11) is obtained. The line charger per unit length on the strip Q is then given by σ', as follows:

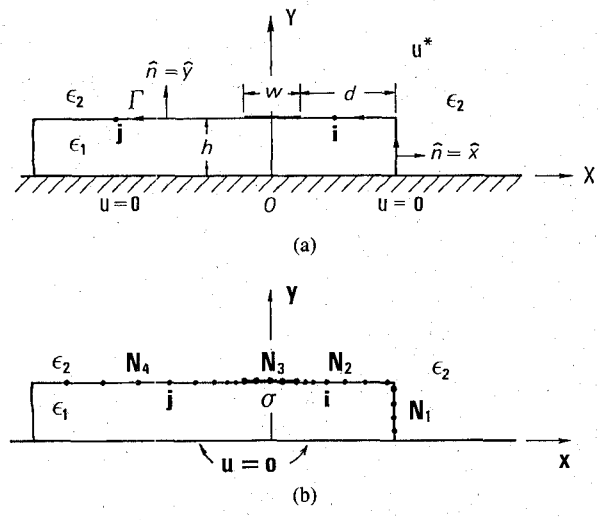

Fig. 4. (a) x–y coordinates for analysis. (b) Division of boundaries.

$$Q = \int_\Gamma \sigma\, d\Gamma = \frac{w}{2}\int_{-\pi/2}^{\pi/2} \sigma'\left(\frac{w}{2}\sin\theta\right) d\theta \tag{13}$$

Therefore the line capacitance C per unit length is given as

$$C = \frac{Q}{V_0} = Q \tag{14}$$

where V_0 is unity. Letting C_0 be the line capacitance of a line per unit length when the dielectric substrate is removed off, the characteristic impedance Z and the phase velocity factor λ/λ_0 of the line under the quasi-TEM approximation are given by the following equations [11]:

$$Z = \frac{1}{v_0\sqrt{CC_0}} \tag{15a}$$

$$\frac{\lambda}{\lambda_0} = \sqrt{\frac{C_0}{C}} \tag{15b}$$

where v_0 is the velocity of light in free space, λ_0 and λ are the wavelength in free space and the guided wavelength of the line, respectively.

IV. Numerical Results

The numerical analysis was first carried out for microstriplines without considering the side-proximity effect in order to show the effectiveness of our method. The numerical results are consistent with the results in other papers as are shown in Table I.

Fig. 5 shows an excellent convergence of the numerical

TABLE I
THE COMPARISON OF THE CHARACTERISTIC IMPEDANCE FOR MSL WITHOUT SIDE-PROXIMITY EFFECT

Parameter of MSL*	Yamashita [3]	Pucel [11]	Yamashita [12]	Schneider [13]	This Theory
$\epsilon_1 = 1.00$, $w/h = 1.0$	126.20	126.61	126.7	126.55(126.60**)	126.43
$\epsilon_1 = 4.20$, $w/h = 0.4$	105.14	—	106.0	—	105.42
$\epsilon_1 = 12.9$, $w/h = 0.240$	74.98	—	—	—	75.00
$\epsilon_1 = 12.9$, $w/h = 0.732$	49.86	—	—	—	50.00

*$\epsilon_2 = 1.0$, **Measured Data.

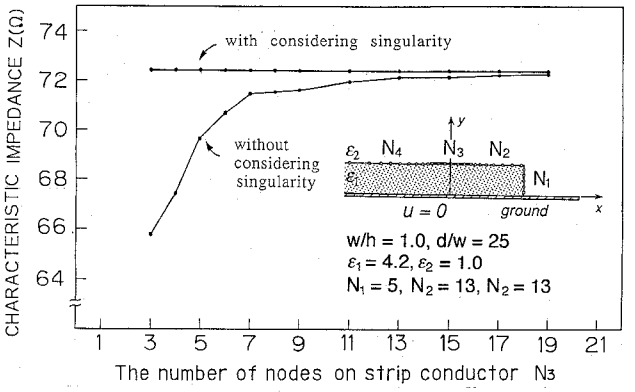

Fig. 5. Convergence of the numerical results for characteristic impedance as a function of the division number on the conductor strip.

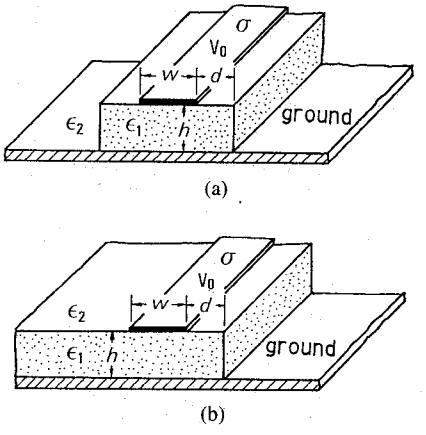

Fig. 6. (a) Symmetrical microstrip-like structure. (b) Asymmetrical microstrip-like structure.

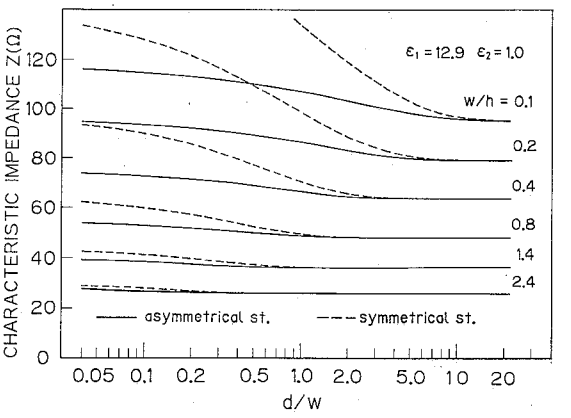

Fig. 7. Side-proximity effect of characteristic impedance taking w/h as a parameter.

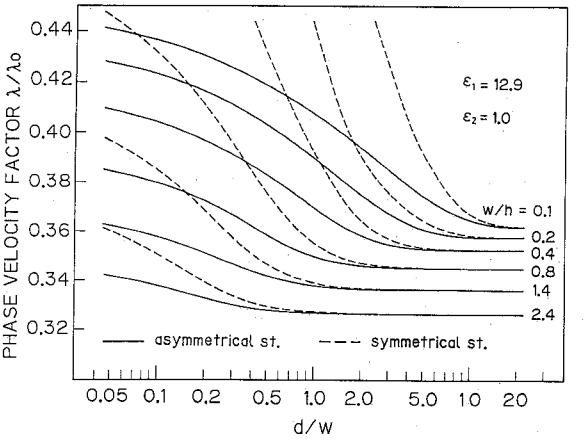

Fig. 8. Side-proximity effect of phase velocity factor λ/λ_0 taking w/h as a parameter.

results for calculating the characteristic impedance as a function of the division number of the conductor strip by removing the singularity when compared with the data without considering the singularity.

The numerical analysis for the structures considering the side-proximity effects are carried out on symmetric and asymmetric microstrip structures as shown in Fig. 6(a) and (b).

Figs. 7 and 8 show the side-proximity effect on the characteristic impedance Z and on the phase velocity factor λ/λ_0 as a function of normalized distance from one side of the substrate d/w. In this calculation, the dielectric constant of substrate $\epsilon_1 = 12.9$ (GaAs) and w/h is taken as a parameter. The solid lines show the results of the asymmetric structure and the dotted lines are for the symmetric one.

Fig. 9 shows the side-proximity effect in the asymmetric structure taking the dielectric constant of the substrate as a parameter.

From these numerical results, both the characteristic impedance and the phase velocity factor are found to be increased by several percent when the conductor strip is approaching to the side of substrate, i.e., d/w becomes approximately unity. But where the strip departs from the side-edge as far as $d/w \geq 3$, the side-proximity effect becomes negligible.

Fig. 10(a) and (b) show the numerical results of the

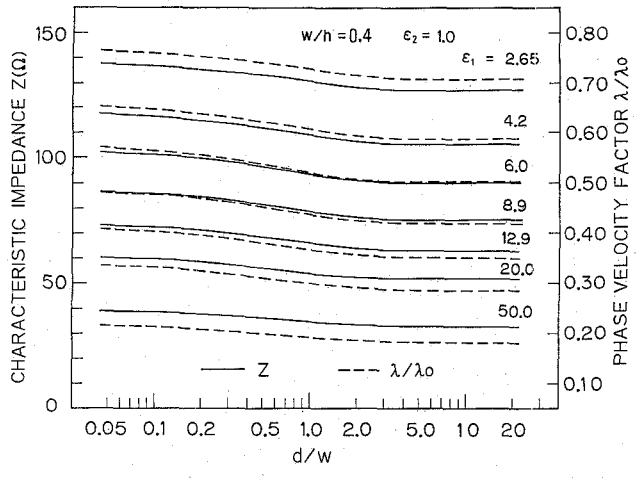

Fig. 9. Side-proximity effects of line characteristics taking dielectric constant of substrate as a parameter.

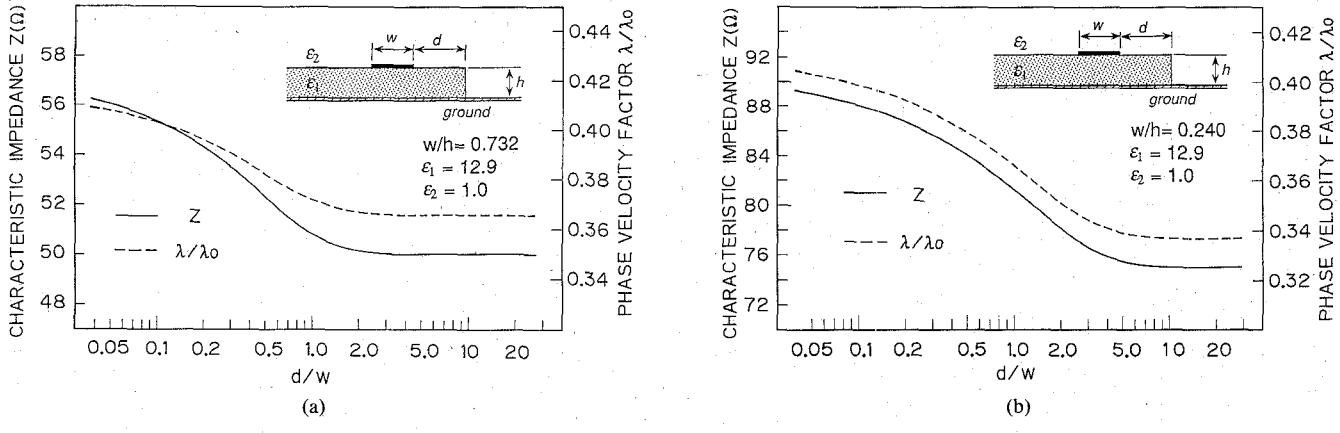

Fig. 10. (a) Side-proximity effects of 50 Ω line. (b) Side-proximity effects of 75 Ω line.

TABLE II
THE COEFFICIENTS OF THE POLYNOMIALS IN (16) BY THE LEAST SQUARE METHOD

Coefficients of the polynomials in (16)	For 50 Ω Lines		For 75 Ω Lines	
	For Z/Z_0	For λ/λ_0	For Z/Z_0	For λ/λ_0
a_0	0.10260	0.35531	0.10795(+1)*	0.38488
a_1	−0.28356(−1)	−0.97956(−2)	−0.51306(−1)	−0.18297(−1)
a_2	0.42473(−2)	0.14674(−2)	0.13565(−2)	0.48318(−3)
a_3	0.81551(−3)	0.27987(−3)	0.22557(−2)	0.80443(−3)

*Numbers in brackets (n) mean exponent: 10^n

side-proximity effect for the 50 Ω and 75 Ω lines widely used in microwave circuits. These results are applicable to the design of MMIC's and to the CAD of MMIC's. The numerical results for the characteristic impedance and the phase velocity factor are also given in the simple polynomials, obtained by the least-squares-method, shown as follows:

$$\frac{Z}{Z_0} \quad \text{or} \quad \frac{\lambda}{\lambda_0} \sum_{j=1}^{3} a_k \left(\ln \frac{d}{w} \right)^k, \tag{16}$$

where the a_k's are the coefficients as shown in Table II. The error of these formulae is less than one percent.

V. CONCLUSION

In this paper, a new method of analysis based on the indirect BEM which can remove the singularity of boundary distribution in the microstrip-like structure is proposed. The side-proximity effect of the microstriplines is analyzed by using this method. From the numerical results, it is found that the characteristic impedance and

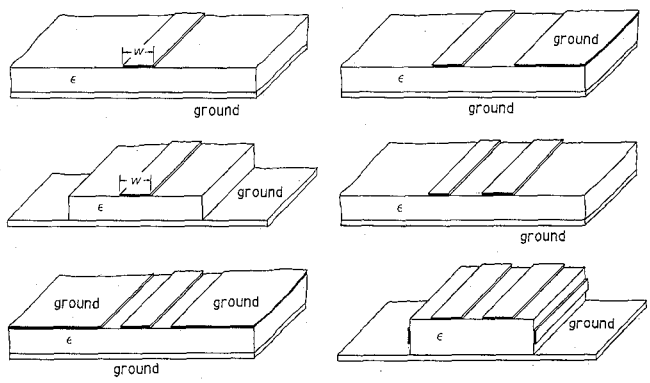

Fig. 11. Various microstrip-like structures which can be analyzed by the method proposed in this paper.

phase velocity factor are considerably affected by the side-proximity effect. The numerical results for 50 Ω and 75 Ω lines are also given in simple polynomial formulas suitable for the CAD of MMIC's.

The analysis proposed here is simple and convenient for the analysis of the microstrip-like structures. It takes only one minute of CPU time on a 16-bit personal computer to obtain a set of results of the characteristic impedance and the phase velocity factor with convergence of less than one percent. This technique is also applicable to various types of microstrip-like structures. For example, it can be applied directly to the analysis of the structures as shown in Fig. 11.

Appendix I
Derivatives of the Analytical Expressions of the Coefficient Matrix Elements $\hat{H}_{ij}$ and $\hat{G}_{ij}$

The elements of coefficient matrices $\hat{H}_{ij}$ and $\hat{G}_{ij}$ from (6) and (7) are given as follows:

$$\hat{H}_{ij} = \frac{l_j}{2}\left\{\int_{\Gamma_{j-1}} \phi_2(\xi)\, q^*\, d\xi + \int_{\Gamma_j} \phi_1(\xi)\, q^*\, d\xi\right\} \tag{A1}$$

$$\hat{G}_{ij} = \frac{l_j}{2}\left\{\int_{\Gamma_{j-1}} \phi_2(\xi)\, u^*\, d\xi + \int_{\Gamma_j} \phi_1(\xi)\, u^*\, d\xi\right\} \tag{A2}$$

where u^* is the fundamental solution, Γ_j is a linear boundary element, l_j is the length of boundary element as shown in Fig. 12 and $\Phi_{1,2}(\xi)$ are linear interpolating functions. For simplicity, the following integrals for the elements are defined as

$$h_{ij}^{(1)} = \frac{l_j}{2}\left\{\int_{\Gamma_j} \phi_1(\xi)\, u^*\, d\xi\right\}, \quad h_{ij}^{(2)} = \frac{l_j}{2}\left\{\int_{\Gamma_j} \phi_2(\xi)\, u^*\, d\xi\right\}, \tag{A3}$$

$$g_{ij}^{(1)} = \frac{l_j}{2}\left\{\int_{\Gamma_j} \phi_1(\xi)\, u^*\, d\xi\right\}, \quad g_{ij}^{(2)} = \frac{l_j}{2}\left\{\int_{\Gamma_j} \phi_2(\xi)\, u^*\, d\xi\right\}. \tag{A4}$$

Thus the integrals in (A1) and (A2) are rewritten as follows:

$$\hat{H}_{ij} = h_{ij-1}^{(2)} + h_{ij}^{(1)}, \quad \hat{G}_{ij} = g_{ij-1}^{2} + g_{ij}^{(1)}. \tag{A5}$$

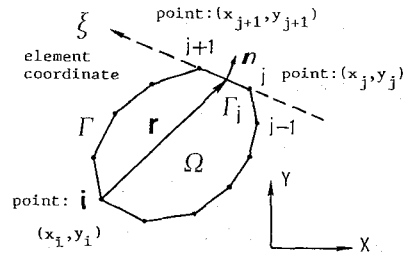

Fig. 12. Division of boundaries and coordinates for analysis.

Because the fundamental solution u^* defined in (5a) and (5b) is expressed as the difference between two natural logarithmic functions with the same form, the integrals defined above in (A3) and (A4) can be derived only for one of these logarithms. The other ones may be found by the same process. Here we choose one of the functions of the fundamental solutions as

$$u^* = \frac{1}{2\pi} \ln \frac{1}{r}. \tag{A6}$$

Then

$$q^* = \frac{\partial u^*}{\partial n} = \frac{1}{2\pi}\frac{R_{ij}}{r^2} \tag{A7}$$

where

$$x = \phi_1(\xi)x_j + \phi_2(\xi)x_{j+1} \tag{A8a}$$

$$y = \phi_1(\xi)y_j + \phi_2(\xi)y_{j+1} \tag{A8b}$$

$$r = \sqrt{(x - x_i)^2 + (y - y_i)^2}$$

$$= \sqrt{(x_S\xi + x_m - x_i)^2 + (y_S\xi + y_m - y_i)^2}$$

$$R_{ij} = \{((x_m - x_i)y_s + (y_m - y_i)(-x_s)\}/(l_j/2)$$

$$x_s = \tfrac{1}{2}(x_{j+1} - x_j), \quad y_s = \tfrac{1}{2}(y_{j+1} - y_j)$$

$$x_m = \tfrac{1}{2}(x_{j+1} + x_j), \quad y_m = \tfrac{1}{2}(y_{j+1} + y_j)$$

in the coordinates as in Fig. 12.

Defining the directional vector and the outward normal vector of linear element Γ_j be $\boldsymbol{l}_j$ and $\boldsymbol{n}_j$, respectively, as shown in Fig. 12, we have

$$\boldsymbol{l}_j = \frac{x_s}{l_j/2}\boldsymbol{x} + \frac{y_s}{l_j/2}\boldsymbol{y}, \tag{A9a}$$

$$n_j = \frac{x_s}{l_j/2}\boldsymbol{x} - \frac{y_s}{l_j/2}\boldsymbol{y}, \tag{A9b}$$

and for simplicity the following variables are defined as

$$\cos\theta = \frac{\boldsymbol{r}_m \cdot \boldsymbol{l}_j}{r_m}, \quad a = \frac{r_m}{l_j/2}$$

$$\boldsymbol{r}_m = (x_m - x_i)\boldsymbol{x} + (y_m - y_i)\boldsymbol{y}$$

$$r_m = |\boldsymbol{r}_m| = \sqrt{(x_m - x_i)^2 + (y_m - y_i)^2}.$$

The integrals in (A3) and (A4) can be analytically obtained and are given as follows:

$$h_{ij}^{(1)(2)} = -\frac{1}{2\pi}\frac{l_j}{4} R_{ij} \int_{-1}^{1} \frac{1 \mp \xi}{r^2}\, d\xi = -\frac{R_{ij}}{2\pi l_j} I_h^{(1)(2)} \tag{A10}$$

$$g_{ij}^{(1)(2)} = -\frac{1}{2\pi}\frac{l_j}{4} \int_{-1}^{1} (1 \mp \xi) \ln r\, d\xi = -\frac{l_j}{8\pi}\left(\ln\frac{l_j}{2} + \frac{1}{2} I_g^{(1)(2)}\right) \tag{A11}$$

where

$$I_h^{(1)(2)} = \int_{-1}^{1} \frac{1 \mp \xi}{\xi^2 + 2a\cos\theta\xi + a^2}\, d\xi = (1 \pm a\cos\theta) I_1 \mp I_2$$

$$I_g^{(1)(2)} = \int_{-1}^{1} \frac{1}{2}(1 \mp \xi) \ln\left\{\frac{l_j}{2}(\xi^2 + 2a\cos\theta\xi + a^2)\right\} d\xi = \ln(1 \mp 2a\cos\theta + a^2) - (2 \pm a\cos\theta) + (1 \pm a\cos\theta)(a\sin\theta)^2 I_1 \pm [(1 \pm a\cos\theta)^2 - (a\sin\theta)^2] I_2 \tag{A13}$$

where I_1 and I_2 are given as follows

$$I_1 = \int_{-1}^{1} \frac{1}{\xi^2 + 2a\cos\theta\xi + a^2}\, d\xi = \frac{1}{|a\sin\theta|}\left\{\tan^{-1}\left(\frac{1 + a\cos\theta}{|a\sin\theta|}\right) - \tan^{-1}\left(\frac{-1 + a\cos\theta}{|a\sin\theta|}\right)\right\} \tag{A14}$$

$$I_2 = \int_{-1}^{1} \frac{\xi + a\sin\theta}{\xi^2 + 2a\cos\theta\xi + a^2}\, d\xi = \ln\frac{\xi^2 + 2a\cos\theta\xi + a^2}{\xi^2 - 2a\cos\theta\xi + a^2}. \tag{A15}$$

When the observation point i' exists in the processed element Γ_j, the latter integrals become singular but they are found by taking their limit as follows:

$$h_{ii}^{(1)(2)} = 0 \tag{A16}$$

$$g_{ij}^{(1)(2)} = \frac{l_j}{8\pi}\left(1 - \ln(l_j) \pm \frac{1}{2}\right). \tag{A17}$$

The integral in (A16) vanishes because the boundary points i considered in the derivation of the boundary integral equation are excluded from the range of integral.

The other integrals in the fundamentals in (5a) can be obtained substituting the image point $i'(x_i - y_i)$ into the expressions by the point $i(x_i, y_i)$ and the elements of the coefficient matrices are given by the difference between these two integrals.

Appendix II
Derivation of the Expressions of the Coefficient Matrix Elements $\hat{G}'_{ij}$ and the Line Charge Q in Unit Length

A. Derivation of $\hat{G}'_{ij}$

$\hat{G}'_{ij}$ is given as $\hat{G}_{ij}$:

$$\hat{G}'_{ij} = \frac{w}{2}\left\{\int_{\Gamma_{j-1}} \phi_2(\theta) u^*\, d\theta + \int_{\Gamma_j} \phi_1(\theta) u^*\, d\theta\right\} \tag{A18}$$

$$g_{ij}'^{(1)} = \frac{w}{2}\left\{\int_{\Gamma_{j-1}} \phi_1(\theta) u^*\, d\theta\right\},$$

$$g_{ij}'^{(2)} = \frac{w}{2}\left\{\int_{\Gamma_j} \phi_2(\theta) u^*\, d\theta\right\} \tag{A19}$$

$$\hat{G}'_{ij} = g_{ij-1}^{(2)} + g_{ij}^{(1)} \tag{A20}$$

where $x = (w/2)\sin\theta$, $dx = (w/2)\cos\theta\, d\theta$, and $\phi_{1,2}(\xi)$ are the interpolating functions of θ which are defined as

$$\phi_1(\theta) = \frac{w}{2l_j}(\sin\theta_{j+1} - \sin\theta) \tag{A21a}$$

$$\phi_2(\theta) = \frac{w}{2l_j}(\sin\theta - \sin\theta_j) \tag{A21b}$$

where w is the width of the strip conductor, l_j is the length of boundary element Γ_j.

Using the coordinates as shown in Fig. 12 in Appendix I and substituting the fundamental solution u^* which is defined in (5) into (A19), we have

$$g_{ij}'^{(1)(2)} = \frac{w^2}{8\pi l_j}\int_{\theta_j}^{\theta_{j+1}} \phi_{1,2}(\theta) \cdot \ln\frac{\sin^2\theta - 2\alpha\sin\theta + \alpha^2 + \beta^2}{\sin^2\theta - 2\alpha\sin\theta + \alpha^2 + \beta'^2}\, d\theta, \tag{A22}$$

where

$$\alpha = \frac{x_i}{w/2}, \quad \beta = \frac{(y - y_i)}{w/2}, \quad \beta' = \frac{(y + y_i)}{w/2}. \tag{A23}$$

The integrals in (A22) are found numerically by the 9-point Gaussian numerical integral method in our paper.

B. Derivation of Line Charge Q in Unit Length

The integral of Q defined in (13) can be considered as a special case of the integral in (A22) and is given as

$$Q = \frac{w}{2}\sum_{j=1}^{N}(s_j^{(1)}\sigma'_j + s_{j+1}^{(2)}\sigma'_{j+1}) \tag{A24}$$

where

$$s_j^{(1)} = \frac{1}{\Delta s_j}\int_{\theta_j}^{\theta_{j+1}} (\sin\theta_{j+1} - \sin\theta)\, d\theta = \frac{\Delta\theta_j}{\Delta s_j}\sin\theta_{j+1} + \frac{\Delta c_j}{\Delta s_j} \tag{A25a}$$

$$s_j^{(2)} = \frac{1}{\Delta s_j} \int_{\theta_j}^{\theta_{j+1}} (\sin\theta - \sin\theta_j)\, d\theta$$

$$= -\frac{\Delta\theta_j}{\Delta s_j} \sin\theta_j + \frac{\Delta c_j}{\Delta s_j} \tag{A25b}$$

and $\Delta\theta$, ΔS and ΔC are given by

$$\Delta\theta_j = \theta_{j+1} - \theta_j \tag{A26a}$$

$$\Delta s_j = \sin\theta_{j+1} - \sin\theta_j \tag{A26b}$$

$$\Delta s_j = \cos\theta_{j+1} - \cos\theta_j. \tag{A26c}$$

ACKNOWLEDGMENT

The authors are very much thankful for the helpful discussions with Professor E. Yamashita and Professor K. Atsuki of the University of Electro-Communications.

REFERENCES

[1] R. A. Pucel, "Design considerations for monolithic microwave circuits," *IEEE Trans. Microwave Theory Tech.*, vol. MTT-29, pp. 513-534, no. 6, June 1981.

[2] R. A. Pucel, "MMIC's, modelling and CAD-where do we go from here?," in *Proc. 16th European Microwave Conf.*, Sept. 1986, pp. 61-70.

[3] E. Yamashita, K. R. Li, and Y. Suzuki, "Characterization method and simple design formulas of MCS lines proposed for MMIC's," *IEEE Trans. Microwave Theory Tech.*, vol. MTT-35, pp. 1355-1362, no. 12, Dec. 1987.

[4] T. Itoh, "Generalized spectral domain method for multiconductor printed lines and its application to turnable suspended microstrip," *IEEE Trans. Microwave Theory Tech.*, vol. MTT-26, pp. 983-987, no. 12, Dec. 1978.

[5] C. A. Brebbia, and S. Walker, "Boundary element techniques in engineering." London: Butterworth & Co., 1980.

[6] S. Kagami and I. Fukai, "Application of boundary-element method to electromagnetic field problems," *IEEE Trans. Microwave Theory Tech.*, vol. MTT-32, pp. 455-461, Apr. 1984, and N. Morita, "Comments on 'Application of boundary-element method to electromagnetic field problems'," *IEEE Trans. Microwave Theory Tech.*, vol. MTT-33, pp. 346-347, Apr. 1985.

[7] K. Yashiro, M. Miyazaki, and S. Ohkawa, "Boundary element method approach to magnetostatic wave problems," *IEEE Trans. Microwave Theory Tech.*, vol. MTT-33, pp. 248-252, Mar. 1985.

[8] K. Yashiro and S. Ohkawa, "Boundary element method for electromagnetic scattering from cylinders," *IEEE Trans. Antennas Propagat.*, vol. AP-33, pp. 383-389, Apr. 1985.

[9] M. Koshiba and M. Suzuki, "Application of the boundary-element method to waveguide discontinuities," *IEEE Trans. Microwave Theory Tech.*, vol. MTT-34, pp. 301-307, 1986.

[10] H. A. El-Mikati, and J. B. Davies, "Improved boundary element techniques for two-dimensional scattering problems with circular boundaries," *IEEE Trans. Antennas Propagat.*, vol. AP-35, pp. 539-544, May 1987.

[11] E. Yamashita and R. Mittra, "Variational method for the analysis of microstrip lines," *IEEE Trans. Microwave Theory Tech.*, vol. MTT-16, pp. 251-256, no. 4, Apr. 1968.

[12] R. A. Pucel, D. J. Messe, and C. P. Hartwig, "Loss in microstrip," *IEEE Trans. Microwave Theory Tech.*, vol. MTT-16, pp. 342-350, no. 6, June 1968.

[13] M. V. Schneider, "Microstrip lines for microwave integrated circuits," *Bell Syst. Tech. J.*, pp. 1421-1444, May-June 1969.

Keren Li, photograph and biography not available at the time of publication.

Yoichi Fujii (M'88), photograph and biography not available at the time of publication.